Fusion Engineering and Design 215 (2025) 114979

Contents lists available at ScienceDirect

Fusion Engineering and Design

journal homepage: www.elsevier.com/locate/fusengdes

Robustness of the E×B MDC prototype design for gyrotrons

Benjamin Ell *, Lukas Feuerstein, Gerd Gantenbein, Stefan Illy, Tobias Ruess, Tomasz Rzesnicki, Sebastian Stanculovic, Manfred Thumm, Jörg Weggen, Chuanren Wu, John Jelonnek

Institute for Pulsed Power and Microwave Technology (IHM), Karlsruhe Institute of Technology (KIT), Kaiserstraße 12, Karlsruhe, 76131, Germany

ARTICLE INFO

Keywords:
Collector
Electron cyclotron resonance heating
Gyrotron

ABSTRACT

The Short-Pulse (SP) *E×B* Multistage Depressed Collector (MDC) prototype developed and built at Karlsruhe Institute of Technology (KIT) is theoretically investigated for its robustness to manufacturing tolerances and non-optimized gyrotron operating scenarios. The tolerance analysis is done based on a parametric definition of the collector electrodes for the optimized gyrotron operation with the KIT 2 MW 170 GHz coaxial-cavity gyrotron. The six most dominant geometrical parameters are considered. The prototype design is then adapted to 5 different gyrotron configurations and operation modes, which include the Wendelstein 7-X (W7-X) Upgrade SP gyrotron for 140 GHz and 105 GHz operation, as well as the coaxial-cavity gyrotron in multi-frequency operation at 136 GHz and 204 GHz (in addition to the nominal operation at 170 GHz) and operation at the second harmonic at 170 GHz. The necessary modifications to the mechanical adaption, the magnetic configuration and electrode potentials are highlighted for promising MDC operation in all cases.

1. Introduction

The demand for new fusion reactors continues to grow, as does the flexibility of their design parameters. Common to the various concepts is the need to maximize the efficiency of the plasma heating systems in order to generate more net power. One of these systems is the Electron Cyclotron Resonance Heating (ECRH) with the gyrotron as its core component. To increase the efficiency with gyrotrons, work started several years ago on the realization of an Multistage Depressed Collector (MDC). For this type of collector, a new technology is needed to separate the electrons based on their kinetic energy, despite their strong confinement to the magnetic field lines. The *E×B* drift concept [1–5] is the most promising concept for the separation of electrons based on their kinetic energy and is already experimentally verified at Peter the Great St. Petersburg Polytechnic University (SPbPU) for a 100 kW-class gyrotron [6].

At Karlsruhe Institute of Technology (KIT), a prototype MDC was developed and built with a cylindrical structure and a helical insulation cut [7–10]. This Short-Pulse (SP) prototype collector is used in this work to demonstrate the robustness of the design with an in-depth tolerance analysis in Section 2. In addition, the same design optimized for the KIT 2 MW 170 GHz coaxial-cavity gyrotron is adapted to various other gyrotrons and the expected performance is demonstrated in Section 3. The commercial simulation tool CST Studio Suite (CST) is used to simulate the trajectories of the spent electron beam, and the direct output of the remaining energy at the point of electron-boundary interaction is used to calculate the collector efficiency.

2. Tolerance analysis of the parametric collector electrodes

The tolerance analysis of the SP MDC prototype geometry is divided into the parametric definition of the geometry in Section 2.1, the tolerance analysis by itself in Section 2.2 and the optimization of the voltage operation point in Section 2.3.

2.1. Parametric definition of the collector electrodes

The first step in the tolerance analysis of the SP MDC prototype is a parametric representation of the helical surface. The helical surface of the first electrode is defined as

$$\begin{aligned} x(u,v) &= (R + d_{\mathrm{helix}} \cdot u) \cdot \sin(v \cdot \theta_{\mathrm{helix}}) \\ y(u,v) &= (R + d_{\mathrm{helix}} \cdot u) \cdot \cos(v \cdot \theta_{\mathrm{helix}}) \\ z(v) &= z_{\mathrm{ExB}} + (h_{\mathrm{ExB}} - h_{\mathrm{helix}}) \cdot v \end{aligned} \tag{1}$$

in a Cartesian coordinate system with the basis vectors x, y and z. Parameters under investigation are the inner electrode radius R, the depth of the helical surface in radial dimension d_{helix} and the azimuthal coverage angle of the helical surface θ_{helix}. The initial axial position of

* Corresponding author.
E-mail address: benjamin.ell@kit.edu (B. Ell).

https://doi.org/10.1016/j.fusengdes.2025.114979
Received 18 November 2024; Received in revised form 28 February 2025; Accepted 17 March 2025
Available online 29 March 2025

the $E\times B$ region z_{ExB}, the height of the $E\times B$ region h_{ExB} and the height of the helical gap h_{helix} are required for the parameterization of the axial z coordinate of the helical surface. The axial distance between the helical surface of the first and second electrode is equal to h_{helix}. The range for the surface parameters u and v is set to [0, 1]. The azimuthal coverage angle of the helical surface is defined as

$$\theta_{helix} = \frac{2\pi}{3} + \theta_{over} - \theta_{straight} \tag{2}$$

with the azimuthal overlap angle of the helical surface θ_{over} due to the extension of the helix and the azimuthal coverage angle of the straight cut $\theta_{straight}$. The division of the complete circular angle of 2π by 3 is done for a collector design with a three-fold helix as it is described in the Refs. [7–10]. The initial electron beam radius in the $E\times B$ region is set to 98 mm, primarily as a compromise in the required magnetic field, and an acceptable size of the collector electrodes and coils. The magnetic field profile in the $E\times B$ region is, according to the desired electron beam radius, constant for the design optimization of the prototype. The electron beam radius at the entrance of the $E\times B$ region must be at the nominal design value. Hence, z_{ExB} is constant for a constant magnetic field profile. The helical depth d_{helix} is not important for electrical performance. However, it must be ensured that the slow electrons are collected on it and do not escape the helical gap. The last parameter for the parametric definition of the SP MDC prototype, which is not included in Eq. (1), is the height of the bottom straight cut $h_{straight}$. All parameters of the geometric study are shown graphical in Fig. 1.

2.2. Tolerance analysis

The design of the SP MDC prototype is achieved with empirical optimization due to the high degree of freedom. However, a systematic parametric investigation of the geometry based on Eq. (1) is performed for validation of the design decisions and tolerance analysis of individual parameters. For simplification of the analysis, only a single parameter is changed at a time with all other parameters at their nominal value. The voltage operating point of the collector is considered constant for the parametric analysis and is based on a theoretical analysis of the spent electron beam. The goal is a maximum $E\times B$ drift, thus potential difference between the electrodes, while the theoretical collector efficiency is at approximately 80%, based on the kinetic energy spectrum of the spent electron beam. The closest voltage tabs of the Power Supply Unit (PSU) at the KIT Fusion Long Pulse Gyrotron Laboratory (FULGOR) test-stand [11] to meet those requirements, while the gyrotron body is at ground potential, are 11.25 kV and 46.125 kV for the first and second electrode, respectively. A depression potential of the first electrode close to the kinetic energy of the slowest electron could introduce two limitations, one related to the voltage depression of the electron beam and the other related to a reduced potential difference between both electrodes.

The results of the parametric investigation are shown in Fig. 2 with values for the collector efficiency and the reflected current. The collector efficiency η_{col} is defined with the power of the decelerated electrons when they intersect with a boundary P_{dec} and the power of the spent electron beam after interaction P_{Sbeam} to

$$\eta_{col} = 1 - \frac{P_{dec}}{P_{Sbeam}} \ . \tag{3}$$

The reflected current is a result of the parasitic behavior of the straight connection of the two helical ends and should be kept to a minimum. Reflected electrons are most likely to return to the cavity where they could gain energy from the electromagnetic wave [12], are reflected again, and are collected at a collector electrode. However, the interaction might be disturbed or parts of the gyrotron might be bombarded for which they are not intended. The reflected current presented in this paper is recorded in the lower launcher region at the boundary of the simulation, as the simulations do not include cavity interactions.

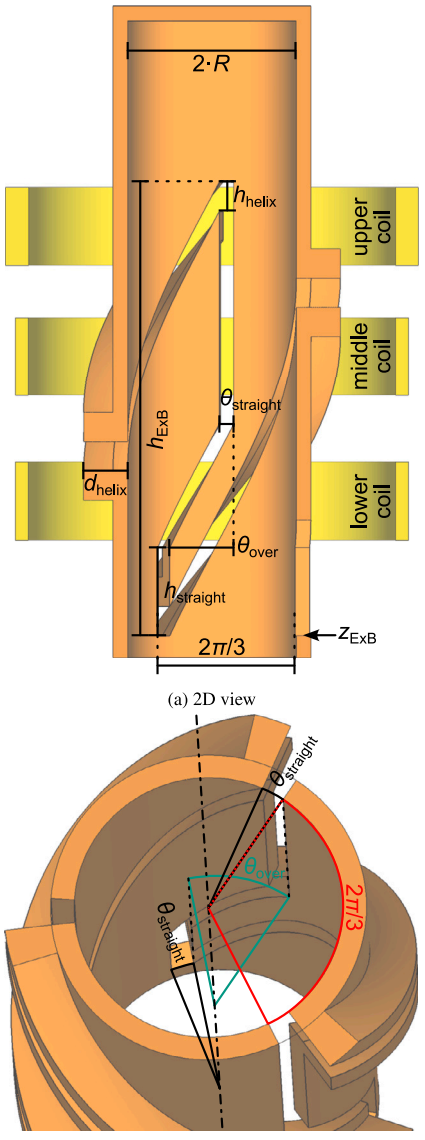

(a) 2D view

(b) 3D view

Fig. 1. Graphical representation of the parametric definition.

In case of the height of the $E\times B$ region h_{ExB} as shown in Fig. 2(a), both, the collector efficiency and the reflected current are increased with reduced height of the $E\times B$ region. For h_{ExB} a compromise is chosen for which the reflected current is acceptable, and the collector efficiency is at an optimum level. This last parameter depends on the voltage operating point of the collector, more specifically, on the difference in the voltages between both electrodes. However, the voltage operating point is considered constant and is investigated in Section 2.3 for the final design.

In case of the inner electrode radius R, as shown in Fig. 2(b), the reflected current increases quickly for a radius larger than the nominal value. For smaller electrode radii, the collector efficiency is decreased, and the sensitivity to misalignment and Stray Magnetic Field (SMF) is increased. This parameter is strongly influenced by the electron beam radius in the $E\times B$ region.

In case of the height of the helical gap h_{helix} as shown in Fig. 2(c), the opposite behavior as for h_{ExB} is observed. A compromise is chosen to limit the reflected current and still achieve an acceptable collector efficiency. On one hand, a minimum distance between both electrodes is required to limit the electric field and to prevent arcing

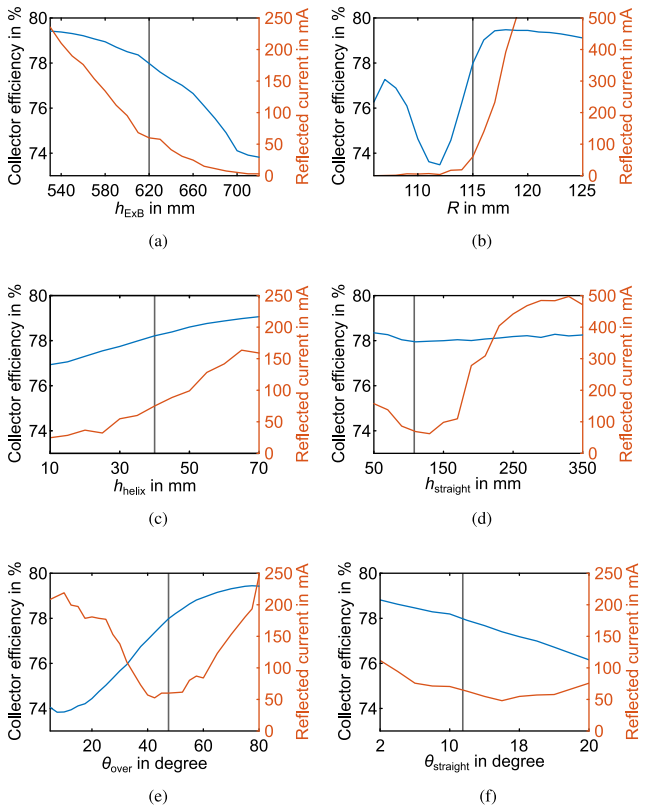

Fig. 2. Parametric analysis for the SP MDC prototype with nominal values marked by gray lines. (a) Variation of the height of the $E{\times}B$ region h_{ExB}, (b) the inner electrode radius R, (c) the height of the helical gap h_{helix}, (d) the height of the bottom straight cut $h_{straight}$, (e) the azimuthal overlap angle of the helical surface θ_{over} and (f) the azimuthal coverage angle of the straight cut $\theta_{straight}$.

during operation. On the other hand, sufficient strength of the electric field is desired to collect the electrons at fixed positions and prevent escaping of (secondary) electrons to the outside.

The height of the bottom straight cut $h_{straight}$ is one of two parameters presented here which are introduced together with the helical extension. The influence of $h_{straight}$ on the performance of the MDC is shown in Fig. 2(d). It can be seen that the reflected current is minimized without a significant influence to the collector efficiency. The azimuthal overlap angle of the helical surface θ_{over} as shown in Fig. 2(e) is the second parameter which is introduced together with the helical extension. Here, a minimization of the reflected current is observed. However, a larger influence on the collector efficiency exists. The influence to the collector efficiency and rising reflected current with increased azimuthal overlap angle is a result of the single parameter observation. With increased overlap, the overall helical slope is decreased, resulting in a similar behavior as a reduced height of the $E{\times}B$ region.

In case of the azimuthal coverage angle of the straight cut $\theta_{straight}$ as shown in Fig. 2(f), a compromise between a low reflected current and high collector efficiency is chosen. In summary, all geometrical parameters are set to a compromise and show a wide resilience against geometrical tolerances. Manufacturing tolerances in the range of mm are uncritical. It can be concluded that all parameters studied are not sensitive to the collector performance and a variation of mm up to cm is acceptable for prototype operation. The most sensitive parameter is the inner electrode radius R which can be compensated with the electron beam radius in the $E{\times}B$ region by modification of the magnetic field in the collector.

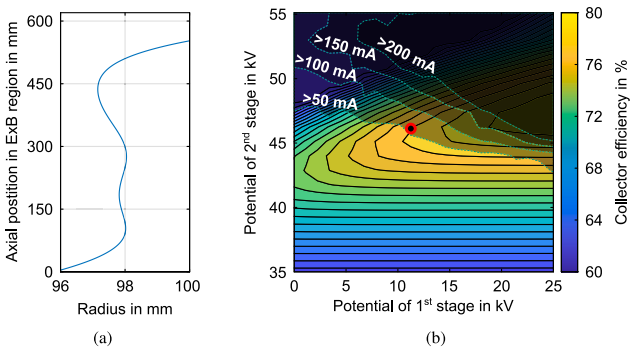

Fig. 3. Analysis of voltage operating point of the optimized MDC prototype geometry. (a) Magnetic field line of the beam center in the $E{\times}B$ region. (b) Simulated collector efficiency with nominal voltage operating point.

2.3. Optimization of the operation point

After parametric analysis of the MDC prototype, an investigation of the different voltage operating points for the fixed geometry is performed. The expected collector efficiency and reflected current are subject to change if the depression potentials are varied. The collector potentials and magnetic field in the collector can be changed during experiments. The magnetic field line of the beam center in the $E{\times}B$ region as shown in Fig. 3(a) is used for the analysis of the collector potentials with the results shown in Fig. 3(b). The range of the axial position of the bottom helix is between 0 mm to 580 mm, while it is between 40 mm to 620 mm for the upper helix. The collector efficiency is represented by equipotential lines while the reflected current is represented with an overlay of a few equipotential lines and shadows. The region below a reflected current of 50 mA is considered safe for operation, while a reflected current above 200 mA should be avoided. The nominal voltage operating point with depression potentials of 11.25 kV and 46.125 kV is not optimal. A slight adjustment of the potentials to 13.5 kV and 45 kV could be considered to increase the collector efficiency to 78.8% and decrease the reflected current to 51 mA. However, it should be noted that the difference in the voltages between both electrodes and with it the strength of the $E{\times}B$ drift is decreased by around 10% by using the more optimal voltage operating point.

3. Adaption of the SP MDC to different gyrotrons

The modular structure of the SP MDC prototype is a promising concept for future modifications of individual subcomponents without the need for reproduction of the complete MDC. Another benefit of the modular design is the adaptability of the MDC to a variety of different gyrotrons that are operated at various frequencies. With increased flexibility of the MDC, an earlier experimental campaign is feasible in case of unavailability of the optimized equipment as other non-optimized components like gyrotrons or magnets can be used for an enlargement of the possible experimental setups.

The flexibility and robustness of the MDC is demonstrated through its adaptation from the KIT 2 MW 170 GHz coaxial-cavity gyrotron to the Wendelstein 7-X (W7-X) Upgrade SP gyrotron for 140 GHz operation in the designated 5.6 T Super Conducting (SC) magnet. However, it is also compatible with 105 GHz operation of the W7-X Upgrade SP gyrotron in a 4.2 T SC magnet, and multi-frequency operation as well as at different harmonics with the KIT 2 MW 170 GHz coaxial-cavity gyrotron. All operation scenarios which are investigated in this work are listed in Table 1 and are described in detail in the following subsections.

Table 1
Operation possibilities of the SP MDC prototype on different gyrotrons.

Sec.	Gyrotron with nominal frequency	Operation frequency	Magnet nominal field	Magnet applied field	Collector beam radius	Total coil current	Lower coil current	Middle coil current	Upper coil current
2.3	2 MW 170 GHz coaxial-cavity	170 GHz	10 T	6.9 T	98 mm	30 kA · t	7.4 kA · t	7.4 kA · t	15.2 kA · t
3.1	1.5 MW 140 GHz W7-X	105 GHz	4.2 T	4.2 T	98 mm 100 mm	24 kA · t 22 kA · t	5.6 kA · t 5.1 kA · t	6.7 kA · t 5.8 kA · t	11.4 kA · t 11.4 kA · t
3.2	1.5 MW 140 GHz W7-X	140 GHz	5.6 T	5.6 T	100 mm	22 kA · t	3.5 kA · t	6.0 kA · t	12.2 kA · t
3.3	2 MW 170 GHz coaxial-cavity	136 GHz	10 T	5.5 T	98 mm	27 kA · t	7.5 kA · t	6.2 kA · t	13.4 kA · t
3.4	2 MW 170 GHz coaxial-cavity	204 GHz	10 T	8.3 T	98 mm	34 kA · t	7.8 kA · t	8.6 kA · t	17.5 kA · t
3.5	2 MW 170 GHz coaxial-cavity	170 GHz	6.87 T	3.5 T	99 mm	17 kA · t	5.1 kA · t	3.0 kA · t	9.3 kA · t

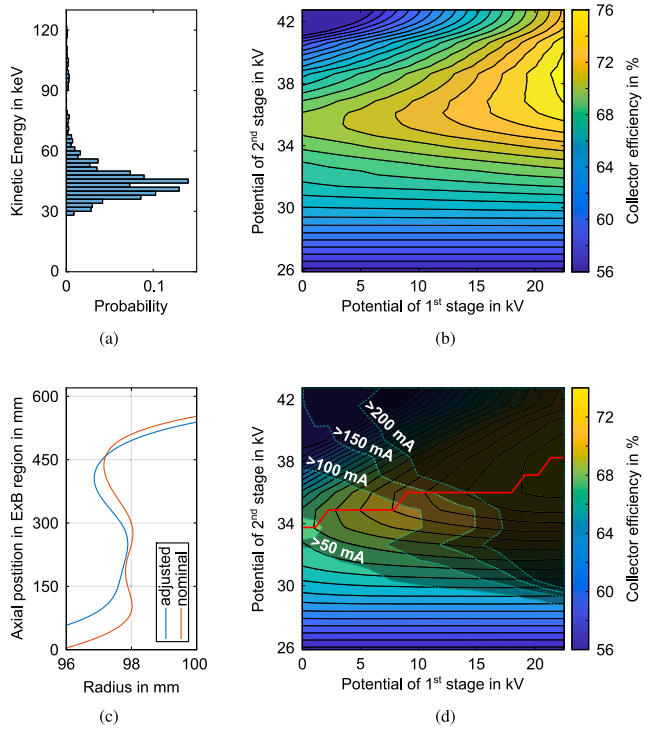

Fig. 4. Adaption of the SP MDC to the W7-X Upgrade SP gyrotron operated in a 4.2 T magnet. (a) Kinetic energy spectrum of the spent electron beam. (b) Theoretical collector efficiency based on the kinetic energy distribution. (c) Magnetic field line of the beam center in the $E\times B$ region. (d) Simulated collector efficiency.

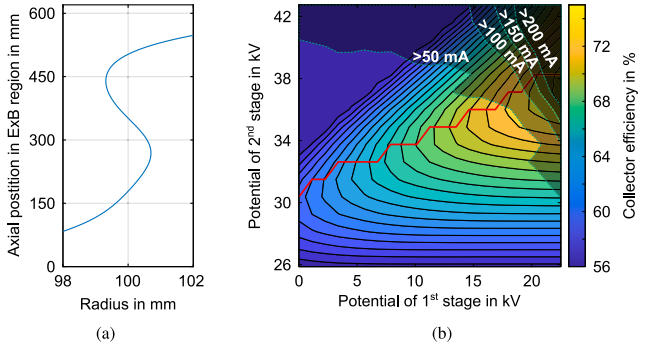

Fig. 5. Optimization of the SP MDC operation with the W7-X Upgrade gyrotron at 105 GHz. (a) Magnetic field line of the beam center in the $E\times B$ region. (b) Simulated collector efficiency.

3.1. Operation of the W7-X SP pre-prototype at 105 GHz

One possibility of SP MDC prototype operation is the adaption to the 1.5 MW 140 GHz W7-X SP pre-prototype gyrotron operated in a 4.2 T SC magnet at a frequency of 105 GHz. The mechanical adaption is possible with a second version of the lower assembly with matching dimensions to the mirror-box, as shown in Ref. [10]. Due to the availability of other suitable magnets, we decided to use this non-optimized mode because it is the first possibility at KIT for MDC verification with a MW-class gyrotron. The operation of the W7-X gyrotron in the 4.2 T magnet is possible however, the operation mode is limited to co-rotating modes with a magnetic field in the positive z-direction. Counter-rotating modes (against the electron rotation) with the same direction of the magnetic field are not possible due to the launcher design of the W7-X gyrotron, while a magnetic field in the negative z-direction is not possible due to the $E\times B$ drift. According to the $E\times B$ drift principle, the same collector geometry cannot be utilized for both magnetic field directions due to the change of drift direction. The majority of electrons would then drift to the inside with exception to the electrons at azimuthal position of the straight gap. An operating point with a less optimized co-rotating mode is chosen therefore to achieve a spread in the kinetic energy distribution of the spent electron beam for MDC experiments, which is shown in Fig. 4(a).

Based on the kinetic energy distribution an analytic investigation is carried out to calculate the maximum collector efficiency at a range of depression potentials applied to both electrodes. The result is shown in Fig. 4(b). In the investigation, reflected currents are neglected, and all electrons are collected with the least kinetic energy remaining. In the regime of a low depression potential of the second electrode, where no electrons are collected at the first electrode, the collector efficiency is not influenced by the potential of the first electrode. As the potential of the second electrode increases, a larger number of electrons is collected at the first electrode. Consequently, the collector efficiency is also influenced by the depression potential of the first stage.

A beam radius in the $E\times B$ region of 98 mm is considered for operation with the W7-X pre-prototype, which is identical to the KIT 2 MW 170 GHz coaxial-cavity gyrotron. The adjusted center line of the beam is shown in Fig. 4(c) and is achieved with the coil currents listed in Table 1. It should be mentioned that a flat beam line as for the nominal case is not achievable with the fixed coil geometry and magnetic field profile of the 4.2 T magnet. The simulated results with a 98 mm beam radius are shown in Fig. 4(d). Unfortunately, the majority of collector voltage operating points show a reflected

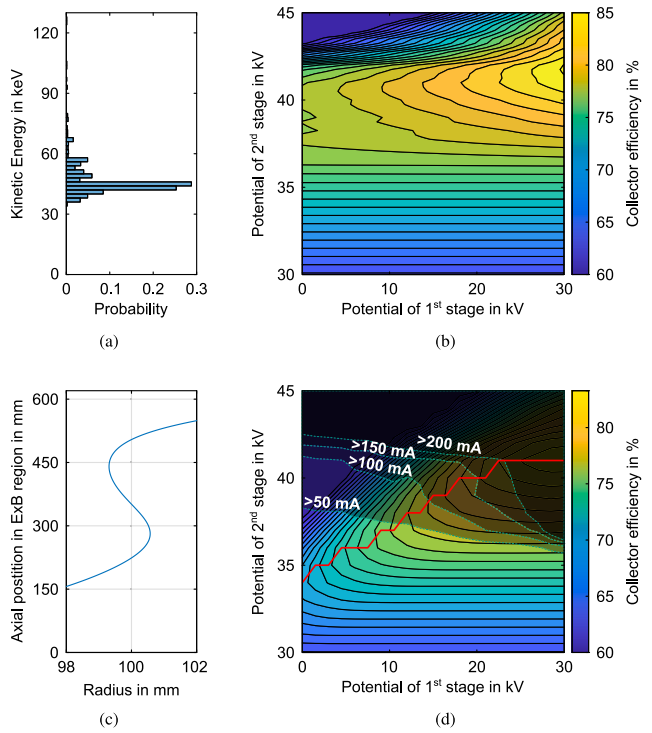

Fig. 6. Adaption of the SP MDC to the W7-X Upgrade SP gyrotron operated at the nominal frequency of 140 GHz. (a) Kinetic energy spectrum of the spent electron beam. (b) Theoretical collector efficiency based on the kinetic energy distribution. (c) Magnetic field line of the beam center in the $E\times B$ region. (d) Simulated collector efficiency.

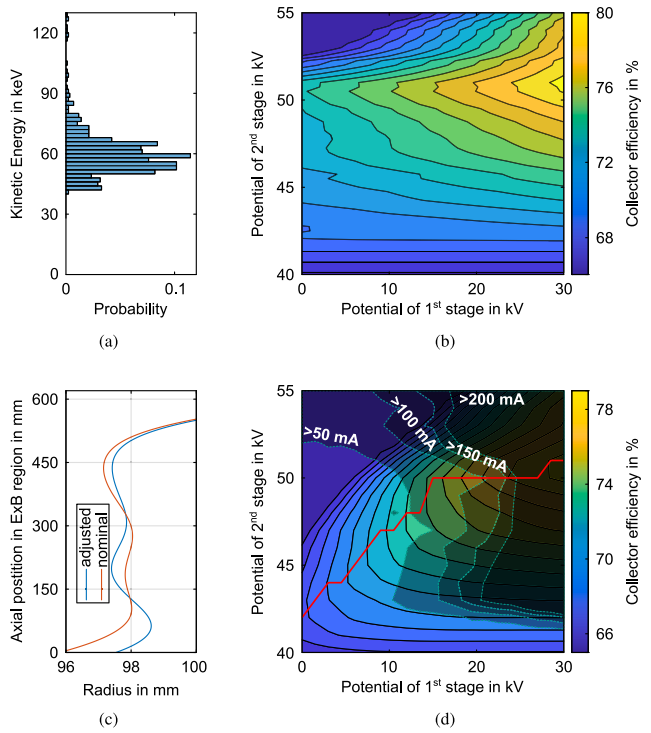

Fig. 7. Adaption of the SP MDC to the 136 GHz coaxial cavity multi-frequency gyrotron operated in the 10 T magnet at KIT. (a) Kinetic energy spectrum of the spent electron beam. (b) Theoretical collector efficiency based on the kinetic energy distribution. (c) Magnetic field line of the beam center in the $E\times B$ region. (d) Simulated collector efficiency.

current above 50 mA and a significant amount reach a reflected current above 200 mA. The expected collector efficiency is limited, as the most promising voltage operating points are probably not achievable in operation. Hence, the operation of the SP MDC with this magnetic field profile is not beneficial and must be optimized.

In order to optimize the magnetic field profile in the collector, it is essential to identify the limiting factor of the previous profile. A fixed potential of the second electrode at a level where the potential of the first electrode does influence the collector efficiency, as indicated by the value of 34 kV, results in an increase in reflected current with the depression potential on the first electrode. In other words, the reflected current is reduced with an increased potential difference between both electrodes. For the case of mechanical optimization, a few options are possible to counteract the weak performance with an increase in the strength of the $E\times B$ drift. However, for electromagnetic optimization, a simple increase in the beam radius solves the issue. The improved magnetic field profile is adjusted to a beam radius of 100 mm, an increase of 2 mm to the nominal operation. The adjusted beam center line from Fig. 5(a) is achieved with the coil currents listed in Table 1. The results with significantly reduced reflected current are shown in Fig. 5(b). Collector efficiencies of 70% to 71.5% are achievable with maximum reflected currents between 50 mA up to 100 mA.

3.2. Operation of the W7-X SP pre-prototype at 140 GHz

The operation of the SP MDC in the W7-X Upgrade SP gyrotron at the nominal frequency of 140 GHz [13–15] is another possibility for MDC experiments at KIT. The gyrotron offers a microwave output power of 1.5 MW with a hollow cavity design and dense kinetic energy spectrum of the spent electron beam as shown in Fig. 6(a). The theoretically calculated collector efficiency based on the kinetic energy spectrum is at high levels for a two stage MDC design as shown in Fig. 6(b). The mechanical adaption of the MDC is identical to Section 3.1.

The critical aspect of adaption of the MDC prototype to the W7-X Upgrade SP gyrotron is the magnetic field profile in the $E\times B$ region due to the faster diverging magnetic field lines of the different magnet and fixed positions of the additional collector coils. A beam center radius of 100 mm is chosen for this investigation as the reflected current of the collector is increased with a beam radius of 98 mm, similar to the operation at 105 GHz. The adjusted beam center line from Fig. 6(c) is achieved with the coil currents listed in Table 1. The simulated collector efficiencies for a variety of collector potentials are shown in Fig. 6(d). A collector efficiency of up to 77% is achievable with a reflected current below 50 mA, while a collector efficiency of 80% is achievable with a reflected current under 150 mA.

3.3. Operation in a coaxial-cavity setup at 136 GHz

The KIT 2 MW 170 GHz coaxial-cavity gyrotron was studied in the past for extension to multi-frequency operation [16]. One of the considered frequencies is 136 GHz with the Transverse Electric $TE_{28,15}$ mode which is co-rotating with the magnetic field in the positive axial direction. A switch to counter-rotating modes with a magnetic field in the negative axial direction is not possible with the fixed geometry of the SP MDC as described earlier and counter-rotating modes with a magnetic field in the positive axial direction would require a new launcher geometry. The advantages of a multi-frequency gyrotron is on one hand the universal application to different kinds of fusion machines and on the other hand, a possibility to modify the heating position in the plasma without moving parts.

Operation of the multi-frequency coaxial-cavity gyrotron at 136 GHz is foreseen in the 10 T SC magnet at KIT in the FULGOR test-stand. No mechanical adaption of the MDC is required due to operation with the nominal gyrotron and magnet. The kinetic energy distribution of the spent electron beam is shown in Fig. 7(a) and the theoretical maximum

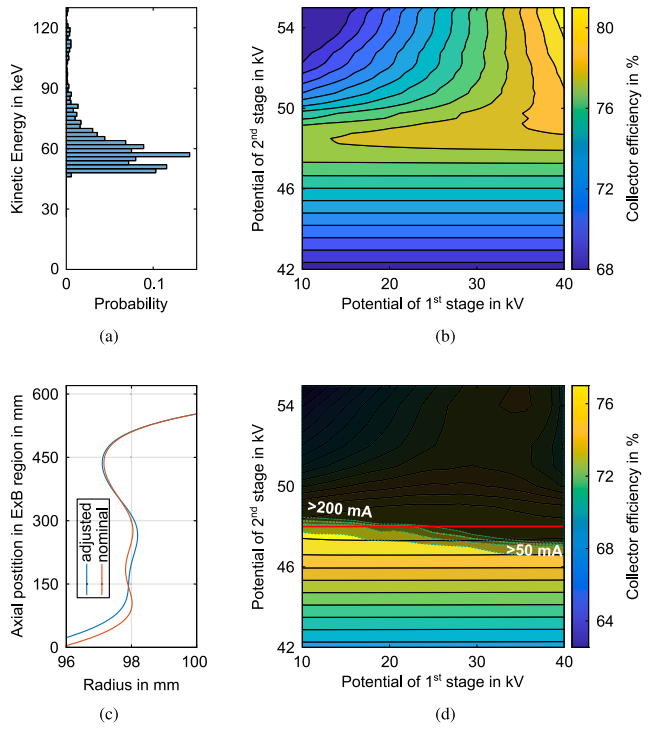

Fig. 8. Adaption of the SP MDC to the 204 GHz coaxial cavity multi-frequency gyrotron operated in the 10 T magnet at KIT. (a) Kinetic energy spectrum of the spent electron beam. (b) Theoretical collector efficiency based on the kinetic energy distribution. (c) Magnetic field line of the beam center in the $E\times B$ region. (d) Simulated collector efficiency.

collector efficiency is shown in Fig. 7(b). The spread in the kinetic energy distribution is higher compared to the nominal operation at 170 GHz and is a limiting factor in the maximum achievable collector efficiency. The identical beam radius of 98 mm as for the nominal operation was chosen for operation at 136 GHz with the beam center line shown in Fig. 7(c). A close match of the beam line to the nominal operation was achieved due to the identical gyrotron magnet which is just operated with different currents. The coil currents are listed in Table 1.

The simulated collector efficiencies for a variety of collector potentials are shown in Fig. 7(d). A collector efficiency of up to 73% is achievable with a reflected current below 50 mA, while a collector efficiency over 77% is achievable with a reflected current below 150 mA.

3.4. Operation in a coaxial-cavity setup at 204 GHz

Similar to the operation of the KIT 2 MW 170 GHz coaxial-cavity gyrotron at 136 GHz multi-frequency operation was studied with extension to 204 GHz [16]. The co-rotating $TE_{40,23}$ mode was chosen as prime candidate for 204 GHz operation of the coaxial-cavity gyrotron due to similar relative caustic radius of the mode compared to the nominal $TE_{34,19}$ mode. Operation is also foreseen in the 10 T SC magnet at KIT in the FULGOR test-stand, which eliminates the need for mechanical adaptation. A major difference of this operation point compared to the other cases are the characteristics of the spent electron beam kinetic energy spectrum as shown in Fig. 8(a). The spectrum is widely spread and has a high probability of the slowest electrons in contrast to the reduced probability of the slowest electrons in other gyrotrons. Such an energy spectrum would require high collector depression potentials in order to achieve a high collector efficiency as shown in Fig. 8(b). However, when both collector potentials of a two-stage collector are close to each other, the strength of the $E\times B$ drift is reduced.

A close match of the beam center line to the nominal operation was achieved due to the identical gyrotron magnet as shown in Fig. 8(c). However, due to the increased magnetic field in the cavity, a higher magnetic field must be also applied in the $E\times B$ region to achieve the desired beam radius of 98 mm, again reducing the strength of the $E\times B$ drift. The coil currents are listed in Table 1 and are significantly higher compared to the other gyrotrons presented in this work.

Despite the limitations of the kinetic energy spectrum and the increased magnetic field in the $E\times B$ region, a collector efficiency of 77% is achievable with a reflected current below 50 mA and is not significantly improved if a higher reflected current is acceptable. All simulated voltage operating points are shown in Fig. 8(d). It can be seen that the most optimum operation points cannot be used with the existing MDC design, due to not strong enough $E\times B$ drift as expected from the theoretical investigation. The electron beam radius in the $E\times B$ region could be increased to increase the depression potential of the first electrode without affecting the reflected current, however, the expected improvement is not high when the theoretical maximum collector efficiency in Fig. 8(b) is considered.

3.5. Operation at higher cyclotron harmonics at 170 GHz

Operation of a vacuum electron tube at the second harmonic of the electron cyclotron resonance frequency is a possibility for reduction of the required magnetic field in the cavity. Until now, high power MW-class gyrotrons are operated at a fundamental mode however, investigations are currently ongoing for a gyrotron operated at the second harmonic with at least 1 MW output power at a frequency above 100 GHz [17–19]. The most significant disadvantage of gyrotron operation at a harmonic mode is a decreased interaction efficiency between the electron beam and the microwave. In order to compensate for this disadvantage, the utilization of an MDC is key to boost the overall tube efficiency to competitive values in comparison to gyrotrons operated at the fundamental frequency.

$$\eta_{\text{total}} = \frac{\eta_{\text{int}} \cdot \eta_{\text{RF}}}{1-(1-\eta_{\text{int}})\cdot\eta_{\text{col}}} \,. \tag{4}$$

As an example, based on Eq. (4) with an efficiency of the Quasi-Optical (QO) system of $\eta_{\text{RF}} = 90\%$ and a collector efficiency of $\eta_{\text{col}} = 80\%$, a total gyrotron efficiency of $\eta_{\text{total}} = 50\%$ is achieved with an interaction efficiency of only $\eta_{\text{int}} = 20\%$. Considering an increased interaction efficiency close to $\eta_{\text{int}} = 25\%$, the total gyrotron efficiency would be at $\eta_{\text{total}} = 56\%$.

At KIT it is currently studied to operate the 2 MW 170 GHz coaxial-cavity SP pre-prototype with slight modifications in the 6.87 T SC magnet at half magnetic field at 170 GHz. Gyrotron operation in the 6.87 T SC magnet is at the moment not foreseen in the FULGOR test-stand due to the cryogenic operation, which would be required for MDC implementation. However, from a physical point of view, there is no limitation, this operation point is the most up-to-date and most promising so far, and no mechanical adaptation of the MDC is required.

The kinetic energy distribution of the spent electron beam is shown in Fig. 9(a) and the theoretical maximum collector efficiency is shown in Fig. 9(b). The minimum kinetic energy is much higher compared to the other gyrotrons shown in this work due to an increased acceleration potential and decreased interaction efficiency which results in increased collector efficiencies compared to fundamental gyrotrons. A beam radius of 99 mm is chosen for the first investigation with the beam line shown in Fig. 9(c). The adjusted beam center line is achieved with the coil currents listed in Table 1.

In simulation, collector efficiencies of up to 85% are achieved with low reflected currents below 50 mA which is close to the theoretical maximum. The results are shown in Fig. 9(d). With reduced magnetic field in harmonic gyrotron operation a different MDC behavior is observed at high potential differences between both electrodes above 30 kV. At such operation points, the $E\times B$ drift is too strong and fast

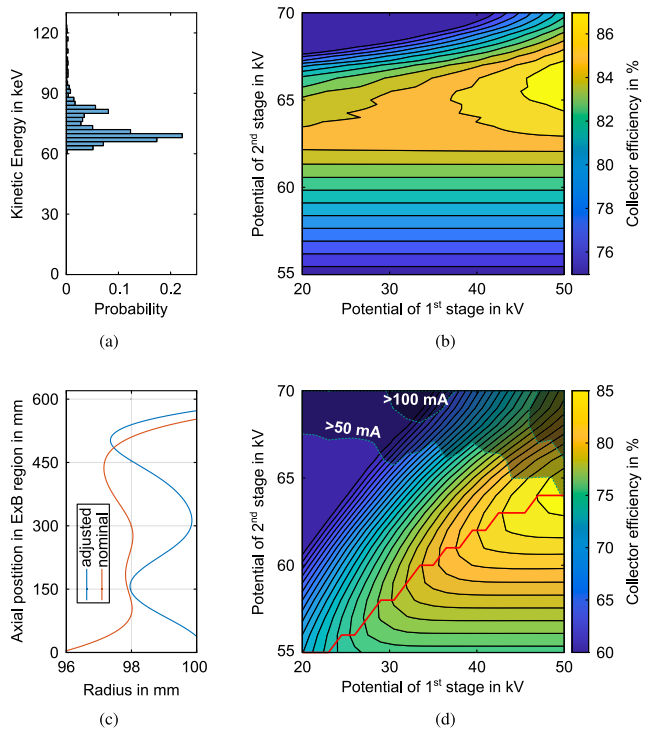

Fig. 9. Adaption of the SP MDC to the 170 GHz coaxial cavity gyrotron operated in the 6.87 T magnet at KIT at the 2nd harmonic. (a) Kinetic energy spectrum of the spent electron beam. (b) Theoretical collector efficiency based on the kinetic energy distribution. (c) Magnetic field line of the beam center in the $E\times B$ region. (d) Simulated collector efficiency for different voltage operating points with different limits for reflected current.

electrons (with kinetic energies above the deceleration potential of the second electrode) are collected at the first electrode with significant remaining energy, thus reducing the collector efficiency and significantly increasing the current collected by the first electrode. In order to operate the SP MDC prototype at such voltage operating points a decreased beam radius could be used with the disadvantage of increased levels of reflected current for the high efficiency operation points.

4. Conclusion

The tolerance analysis of the SP $E\times B$ MDC prototype developed and built at KIT shows a robust behavior of the MDC to geometrical variations of mm up to cm with still acceptable operation performance. Even after optimization to a specific voltage operating point, a slight adjustment of the depression potentials can improve the performance of the MDC on the KIT 2 MW 170 GHz coaxial-cavity gyrotron. For all other gyrotrons studied in this paper, it is possible to operate the SP MDC prototype with adjustments in the current of the additional collector coils and the depression potentials of both collector stages in a wide range of voltage operating points.

CRediT authorship contribution statement

Benjamin Ell: Writing – review & editing, Writing – original draft, Visualization, Validation, Software, Resources, Project administration, Methodology, Investigation, Funding acquisition, Formal analysis, Data curation, Conceptualization. **Lukas Feuerstein:** Resources, Writing – review & editing. **Gerd Gantenbein:** Supervision, Writing – review & editing. **Stefan Illy:** Supervision, Writing – review & editing. **Tobias Ruess:** Resources, Writing – review & editing. **Tomasz Rzesnicki:** Supervision, Writing – review & editing. **Sebastian Stanculovic:** Writing – review & editing. **Manfred Thumm:** Writing – review & editing. **Jörg Weggen:** Conceptualization. **Chuanren Wu:** Writing – review & editing. **John Jelonnek:** Supervision, Writing – review & editing.

Declaration of competing interest

The authors declare that they have no known competing financial interests or personal relationships that could have appeared to influence the work reported in this paper.

Acknowledgments

This work has been carried out within the framework of the EUROfusion Consortium, funded by the European Union via the Euratom Research and Training Programme (Grant Agreement No 101052200 — EUROfusion). Views and opinions expressed are however those of the author(s) only and do not necessarily reflect those of the European Union or the European Commission. Neither the European Union nor the European Commission can be held responsible for them.

Data availability

The data that has been used is confidential.

References

[1] I.Gr. Pagonakis, J.-P. Hogge, S. Alberti, K.A. Avramides, J.L. Vomvoridis, A new concept for the collection of an electron beam configured by an externally applied axial magnetic field, IEEE Trans. Plasma Sci. 36 (2008) 469–480, http://dx.doi.org/10.1109/TPS.2008.917943.

[2] I.Gr. Pagonakis, C. Wu, S. Illy, J. Jelonnek, Multistage depressed collector conceptual design for thin magnetically confined electron beams, Phys. Plasmas 23 (2016) 043114, http://dx.doi.org/10.1063/1.4947565.

[3] C. Wu, I.G. Pagonakis, S. Illy, G. Gantenbein, M. Thumm, J. Jelonnek, Comparison between controlled non-adiabatic and $E\times B$ concepts for gyrotron multistage depressed collectors, EPJ Web Conf. 149 (2017) 04005, http://dx.doi.org/10.1051/epjconf/201714904005.

[4] V.N. Manuilov, M.V. Morozkin, O.I. Luksha, M.Y. Glyavin, Gyrotron collector systems: Types and capabilities, Infrared Phys. Technol. 91 (2018) 46–54, http://dx.doi.org/10.1016/j.infrared.2018.03.024.

[5] B. Ell, I.Gr. Pagonakis, C. Wu, M. Thumm, J. Jelonnek, Coaxial multistage depressed collector design for high power gyrotrons based on $E\times B$ concept, Phys. Plasmas 26 (2019) 113107, http://dx.doi.org/10.1063/1.5118338.

[6] O.I. Louksha, A.G. Malkin, P.A. Trofimov, First experiments on multistage energy recovery in a 4-mm wavelength gyrotron, IEEE Electron Device Lett. 45 (2024) 1638–1641, http://dx.doi.org/10.1109/LED.2024.3424661.

[7] C. Wu, I.Gr. Pagonakis, K.A. Avramidis, G. Gantenbein, S. Illy, M. Thumm, J. Jelonnek, Gyrotron multistage depressed collector based on $E\times B$ drift concept using azimuthal electric field. I. Basic design, Phys. Plasmas 25 (2018) 033108, http://dx.doi.org/10.1063/1.5016296.

[8] C. Wu, I.Gr. Pagonakis, D. Albert, K.A. Avramidis, G. Gantenbein, S. Illy, M. Thumm, J. Jelonnek, Gyrotron multistage depressed collector based on $E\times B$ drift concept using azimuthal electric field. II: Upgraded designs, Phys. Plasmas 26 (2019) 013108, http://dx.doi.org/10.1063/1.5078861.

[9] B. Ell, C. Wu, G. Gantenbein, S. Illy, M.S. Misko, I.Gr. Pagonakis, J. Weggen, M. Thumm, J. Jelonnek, Toward the first continuous wave compatible multistage depressed collector design for high power gyrotrons, IEEE Trans. Electron Devices 70 (2023) 1299–1305, http://dx.doi.org/10.1109/TED.2023.3234885.

[10] B. Ell, C. Wu, L. Feuerstein, G. Gantenbein, S. Illy, T. Ruess, T. Rzesnicki, S. Stanculovic, M. Thumm, J. Weggen, J. Jelonnek, Fabrication and assembly of the gyrotron multi-stage depressed collector prototype at KIT, EPJ Web Conf. 313 (2024) 04006, http://dx.doi.org/10.1051/epjconf/202431304006.

[11] M. Schmid, J. Franck, P. Kalaria, K.A. Avramidis, G. Gantenbein, S. Illy, J. Jelonnek, I.Gr. Pagonakis, T. Rzesnicki, M. Thumm, Gyrotron development at KIT: FULGOR test facility and gyrotron concepts for DEMO, Fusion Eng. Des. 96–97 (2015) 589–592, http://dx.doi.org/10.1016/j.fusengdes.2015.03.003.

[12] K. Sakamoto, M. Tsuneoka, A. Kasugai, T. Imai, T. Kariya, K. Hayashi, Y. Mitsunaka, Major improvement of gyrotron efficiency with beam energy recovery, Phys. Rev. Lett. 73 (1994) 3532–3535, http://dx.doi.org/10.1103/PhysRevLett.73.3532.

[13] K.A. Avramidis, T. Ruess, F. Mentgen, J. Jin, D. Wagner, G. Gantenbein, S. Illy, C. Ioannidis, H.P. Laqua, I.G. Pagonakis, T. Rzesnicki, M. Thumm, R.C. Wolf, J. Jelonnek, Studies towards an upgraded 1.5 MW gyrotron for W7-X, EPJ Web Conf. 203 (2019) 04003, http://dx.doi.org/10.1051/epjconf/201920304003.

[14] K.A. Avramidis, Z.C. Ioannidis, G. Aiello, P. Bénin, I. Chelis, A. Dinklage, G. Gantenbein, S. Illy, J. Jelonnek, J. Jin, H.P. Laqua, A. Leggieri, F. Legrand, A. Marek, S. Marsen, I.G. Pagonakis, T. Ruess, T. Rzesnicki, T. Scherer, D. Strauss, M. Thumm, I. Tigelis, D. Wagner, J. Weggen, R.C. Wolf, Towards a 1.5 MW, 140 GHz gyrotron for the upgraded ECRH system at W7-X, Fusion Eng. Des. 164 (2021) 112173, http://dx.doi.org/10.1016/j.fusengdes.2020.112173.

[15] T. Rzesnicki, K.A. Avramidis, I. Chelis, G. Gantenbein, S. Illy, Z.C. Ioannidis, J. Jin, M. Thumm, J. Jelonnek, 1.5 MW, 140 GHz gyrotron for W7-X - development status and experimental results, in: 2022 47th International Conference on Infrared, Millimeter and Terahertz Waves, IRMMW-THz, 2022, pp. 1–2, http://dx.doi.org/10.1109/IRMMW-THz50927.2022.9896025.

[16] T. Ruess, First 2 MW-Class (136)/170/204 GHz Multi-Frequency Gyrotron Pre-Prototype for DEMO: Design, Construction and Key Components Verification (Ph.D. thesis), Karlsruher Institut für Technologie (KIT), 2023, http://dx.doi.org/10.5445/KSP/1000160391.

[17] K.A. Avramides, C.T. Iatrou, J.L. Vomvoridis, Design considerations for powerful continuous-wave second-cyclotron-harmonic coaxial-cavity gyrotrons, IEEE Trans. Plasma Sci. 32 (2004) 917–928, http://dx.doi.org/10.1109/TPS.2004.828781.

[18] L. Feuerstein, A. Marek, C. Wu, S. Illy, M. Thumm, J. Jelonnek, Design of a second harmonic MW-level coaxial gyrotron cavity, in: 2023 24th International Vacuum Electronics Conference, IVEC, 2023, pp. 1–2, http://dx.doi.org/10.1109/IVEC56627.2023.10156958.

[19] S. Illy, K.A. Avramidis, I. Chelis, B. Ell, L. Feuerstein, G. Gantenbein, Z. Ioannidis, J. Jelonnek, J. Jin, G. Latsas, A. Marek, D. Peponis, T. Rzesnicki, M. Thumm, I. Tigelis, C. Wu, Progress in the design of megawatt-class fusion gyrotrons operating at the second harmonic of the cyclotron frequency, in: 2023 48th International Conference on Infrared, Millimeter, and Terahertz Waves, IRMMW-THz, 2023, pp. 1–2, http://dx.doi.org/10.1109/IRMMW-THz57677.2023.10299170.